Materials Research. 2019; 22(suppl. 1): e20180869
DOI: http://dx.doi.org/10.1590/1980-5373-MR-2018-0869

Ecap Consolidation and Heat Treatment of Blended Elemental Powders of Iron, Chromium, Nickel and Manganese

***Ricardo Sanson Namur*[a]*, *Lorena Moraes Feitosa*[a], *Ana Carolina Krapp Ferreira*[a],**

***Arthur Gustavo Bueno*[b], *Kahl Dick Zilnyk*[b], *Osvaldo Mitsuyuki Cintho*[a]**

[a]*Departamento de Engenharia de Materiais, Universidade Estadual de Ponta Grossa, Av. Carlos Cavalcanti, 4748, Campus Universitário de Uvaranas, 84030-900, Ponta Grossa, PR, Brasil*
[b]*Instituto Tecnológico de Aeronáutica, Departamento de Materiais e Processos, Praça Marechal Eduardo Gomes, 50, Vila das Acacias, 12228-900, São José dos Campos, SP, Brasil*

Received: December 12, 2018; Revised: September 2, 2019; Accepted: December 5, 2019

Equal channel angular pressing (ECAP) is one of the severe plastic deformation processes that can also be used for metallic powder consolidation. Consolidation of blended elemental powders of iron, chromium, nickel, and manganese (Fe-25Cr-20Ni-2Mn wt. %) was performed at room temperature in a $\Phi = 120°$ die by 1 and 2 passes. SEM micrographs indicated that single pass ECAP consolidated sample presented close to full densification. Additional pass of ECAP led to hardness increase and to an apparent better mixing between the different particles. SEM/EDX analysis made before and after heat treatment of the samples showed that effective diffusion only took place after heat treatment and especially in the sample subjected to 2 ECAP passes. Results indicate that alloying by ECAP consolidation and posterior heat treatment is feasible, especially for systems that cannot be processed by conventional means, as well as mechanical alloying.

Keywords: *Powder consolidation, equal channel angular pressing (ECAP), powder metallurgy.*

1. Introduction

Severe plastic deformation (SPD) is commonly defined as processes that ultra-large plastic strains are applied to a bulk material, with no considerable change in its dimensions, and capable of producing ultrafine grained (UFG) metals[1-4]. Several SPD processes were developed, though some have acquired more relevance, as high pressure torsion (HPT)[5], accumulative roll-bonding[6] and, especially, equal channel angular pressing (ECAP)[7-12].

Bulk solid metals are the most commonly discussed materials in ECAP literature, especially aluminum and its alloys. The potential of grain refinement and improvement on the mechanical properties of these materials was reported many times on literature. Manjunath and collaborators presented good results on the ECAP processing of alloys of the system Al-Zn-Mg, with major grain size reduction and simultaneous improvement in the mechanical properties, like hardness, ultimate tensile strength and elongation[13, 14].

ECAP consolidation of metallic powders[15-17] and metal matrix composites[18] have been studied in the last years. Powder metallurgy is the usual method for obtaining bulk solids from powders and its densification mechanisms usually consists in uniaxial pressing, which may not be effective, and mass transfer by atomic diffusion during sintering. ECAP consolidation, on the other hand, has its densification mechanism based on plastic deformation of particles, which may result in almost full densification even in low temperatures and almost instantly[16]. Figure 1 displays a schematic illustration of the consolidation of dissimilar particles by ECAP.

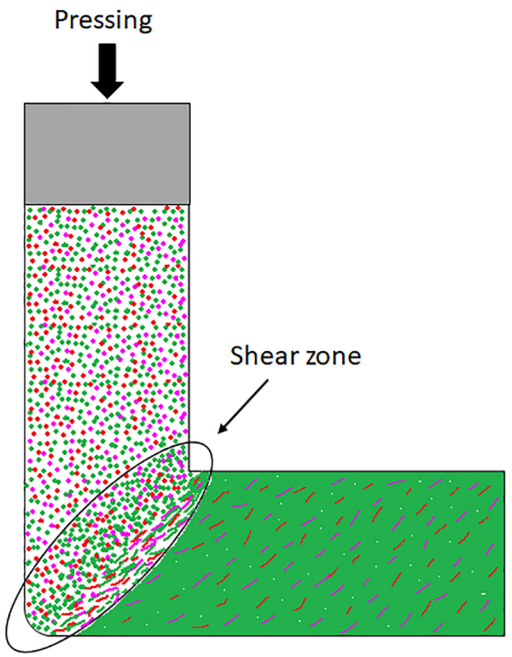

Figure 1. Schematic representation of the consolidation of dissimilar particles by ECAP.

Additionally, densification of metals by sintering is widely known[19] to be negatively affected by the surface oxide layers, reducing the effectiveness of mass transfer in these interfaces. During ECAP consolidation, the metallic

*e-mail: ricardonamur@hotmail.com.

particles are exposed to severe plastic deformation, fracturing the surface oxide layer. This metal surfaces created by the broken oxides are prone to easily bond to other metallic surfaces, which are widely available after SPD[16].

Thus, ECAP consolidation of powders comes up as a great alternative for conventional powder metallurgy processes, once it does not require high sintering temperatures and can be readily performed, reducing energy expenditure and the final cost of the product.

The majority of works in the literature focus on the consolidation of elemental[20-23] or pre-alloyed[24-26] powders. In this research, the consolidation of blended elemental powders of Fe, Cr, Ni, Mn was performed, by ECAP, to investigate the potentiality of obtaining an alloy from this technique. Scanning electron microscopy (SEM) coupled with energy dispersive spectroscopy (EDX) was used for determining the occurrence of diffusion and chemical homogenization. Hardness tests were performed to evaluate the mechanical properties of the samples and the work hardening evolution after 1 and 2 ECAP passes and heat treatment.

2. Experimental

Elemental powders of iron (99.5%), chromium (99%), nickel (99.8%) and manganese (99.7%) in a ratio of Fe-25Cr-20Ni-2Mn wt. % were mechanically blended (without grinding) and simply poured into the entrance channel, without encapsulation, for ECAP consolidation. The chosen elements and its ratio are the same as the AISI 310 stainless steel, which is widely known for its corrosion resistance at high temperatures. Nevertheless, checking the efficiency of the consolidation of diverse metallic particles was the main objective.

Consolidation was performed at room temperature in a sliding bottom die with channel angle of 120° and arc of curvature (Ψ angle) of ≈ 20°. The sliding bottom die has the advantage of diminishing the friction between the die and the part being pressed, as can be seen in Figure 2, where SB is a sliding bottom die and CD is a conventional die. As the material flows through the exit channel, the bottom bar slides and eases the process without deleterious influence on the deformation of the material. Pressing speed was kept at 1 $mm.min^{-1}$, in order to prevent substantial heating of the sample[27]. Samples were obtained by a single pass and by two passes in route A. In order to contain the powder and apply an effective backpressure, a small billet of AISI 1045 was used as dummy billet. To remove the consolidated sample and prepare the die for the second pass, a billet of AISI 1045 was pressed halfway the channel. Heat treatment in both samples was performed under vacuum at 1200 °C for 60 minutes.

To verify the efficacy of the densification by ECAP and heat treatment, the volumetric fraction of porosities was measured by means of automated image analysis, accordingly to the ASTM E1245-03 standard[28].

Samples were analyzed by SEM and optical microscopy (OM) in order to verify the particle deformation behavior during ECAP. SEM-EDX was performed to identify particle interfaces and its chemical composition qualitatively. SEM-EDX line scans were performed for the better visualization of the chemical composition gradient along the interfaces between particles. The obtained billets were cut along its longitudinal-section and conventional metallographic preparation was performed with sandpaper (420, 600, 1200, 1500, 2000, 2500) and vibrational polishing with colloidal silica for 4 hours.

The mechanical behavior of the samples was analyzed by Vickers hardness tests. To understand the behavior of each powder, Vickers hardness measurements were performed on individual particles of the powder prior to the consolidation and after each pass. By this method, it was possible to analyze the hardening of each powder due to the shearing deformation

Figure 2. Picture of a sliding bottom die (SB) and a conventional die (CD) used for ECAP.

imposed by ECAP. Indentations were performed using very low loads, for ensuring that single particles were analyzed (15 gf for Fe and Ni, 50 gf for Cr and Mn). Twenty indentations were obtained for each material, during 12 seconds each.

3. Results and Discussion

3.1 Powder characterization

Characterization of the initial powders was performed by means of SEM and their morphologies can be observed in Figure 3. The SEM images were used to determine the maximum Feret's diameter, which is the longest dimension from edge to edge of a particle. A minimum of 200 measurements were performed for each material. Iron (Figure 3A) and nickel (Figure 3C) (58.5 ± 19.6 µm; 12.1 ± 5 µm; respectively) presented smaller particles with a rounded shape. Some aggregates can be observed, especially for iron, which may have increased the average value of particle size and its deviation. Fewer aggregates were observed for nickel. Chromium (Figure 3B) presented an angular particle shape with much larger size (449.6 ± 78.8 µm) than iron and nickel. Manganese presented irregular shaped particles with a bimodal particles size distribution (17.1 ± 4.6 µm for the smaller ones and 82.3 ± 25.7 µm for the larger ones) as can be seen in Figure. 3D.

3.2 Powder consolidation

The "stress x displacement" curves obtained during ECAP consolidation are shown in Figure 4. The first powder consolidation pass was characterized by an initial compression, where inter-particle sliding and plastic deformation of powder particles took place, analogously to uniaxial pressing. As a critic stress was reached, the compacted powder mass starts to push forward the backpressure dummy billet and to be pressed along the channel, resulting in severe plastic deformation by shear.

The second pass presents a different behavior, with a rapid increase in stress until a critic stress is reached. Then, the sample undergo a steady state of pressing along the channel. The higher stress for the pressing of the second pass can be associated with the strain-hardening during the first pass, making the sample more resistant to the shear deformation imposed by ECAP[26].

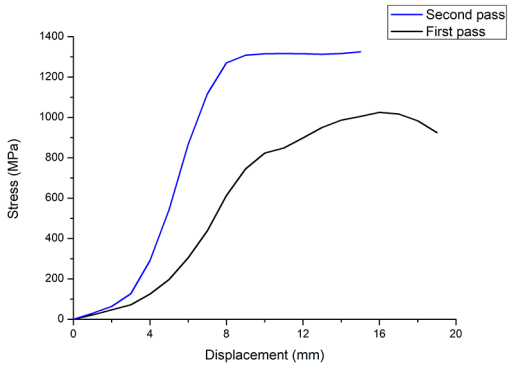

Figure 4. "Stress x displacement" curves obtained for the first and second ECAP passes.

3.3 Microstructure characterization

Figures 5 and 6 present the SEM/OM micrographs obtained for the samples subjected to one and two passes, respectively, before heat treatment. Red arrows indicate the extrusion direction. After the first pass, the sample presents a dense structure, with well-defined interfaces between particles (Figure 5). This result reinforces that SPD by ECAP is an effective tool for obtaining instantaneous highly dense, homogeneous bulk solids. Figures 7 and 8 present the SEM/OM micrographs for the samples after heat treatment. As seen in the SEM images (Figures 7B and 8B), the interfaces between particles became blurry, an indicative of interdifussion[16].

Automated image analysis was performed to quantify the porosity and results are displayed on Table 1. As seen on Table 1, high densification was obtained with a single ECAP pass and it was further improved with the second pass, which may indicate the improvement of the metal-metal bonding between particles. The densification of the samples was also improved by the heat treatment. ECAP densification is mainly based on plastic deformation of particles, whereas sintering is mainly a diffusion based process[16].

3.4 SEM-EDX analysis

SEM-EDX maps were obtained for both samples, before and after heat treatment, and are shown in Figure 9 to Figure 12. SEM-EDX for Mn was not considered, due to the possible misinterpretation between Mn $K\alpha_1$ (5.900 keV) and Cr $K\beta_1$ (5.947 keV).

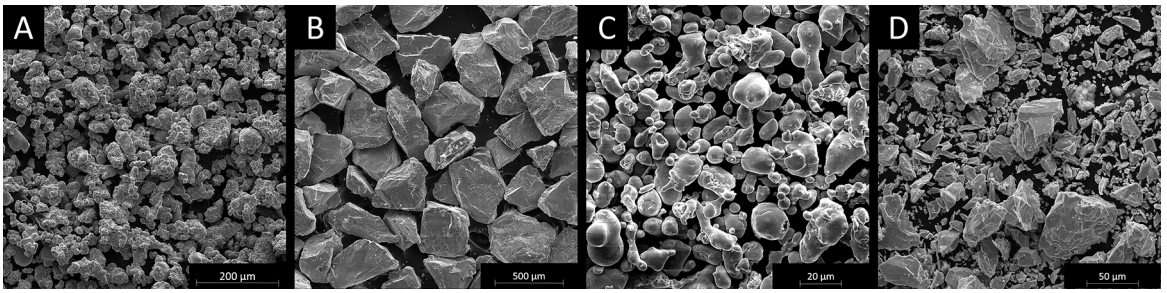

Figure 3. SEM images of the iron (A), chromium (B), nickel (C) and manganese (D) powders used.

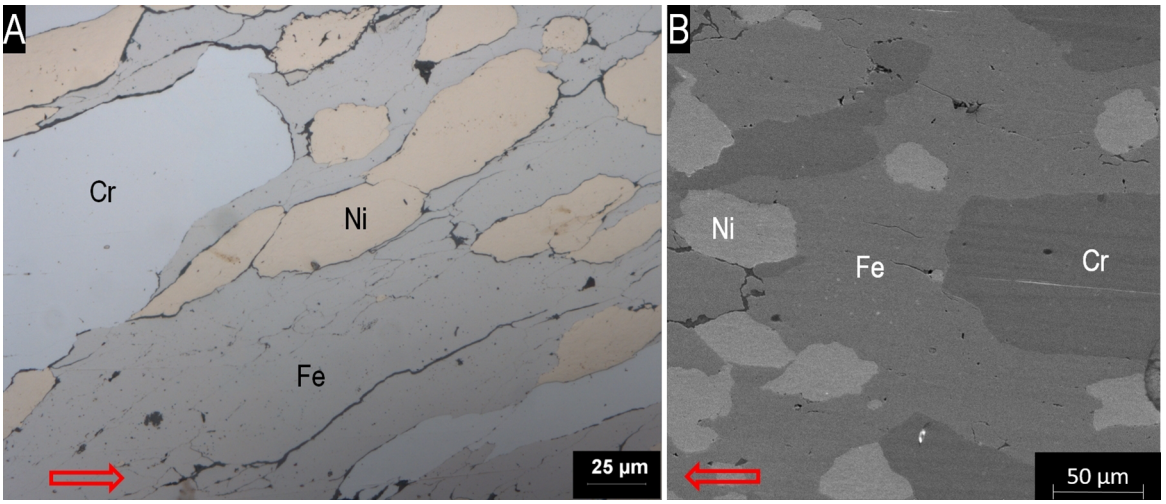

Figure 5. Optical (A) and electron (B) microscopy micrographs for the sample subjected to one ECAP pass, before heat treatment.

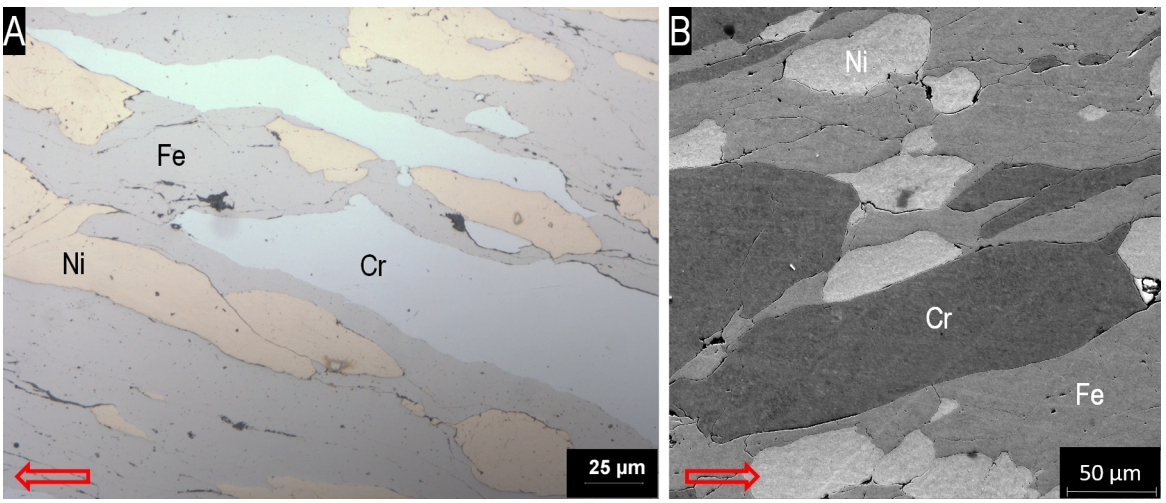

Figure 6. Optical (A) and electron (B) microscopy micrographs for the sample subjected to two ECAP passes, before heat treatment.

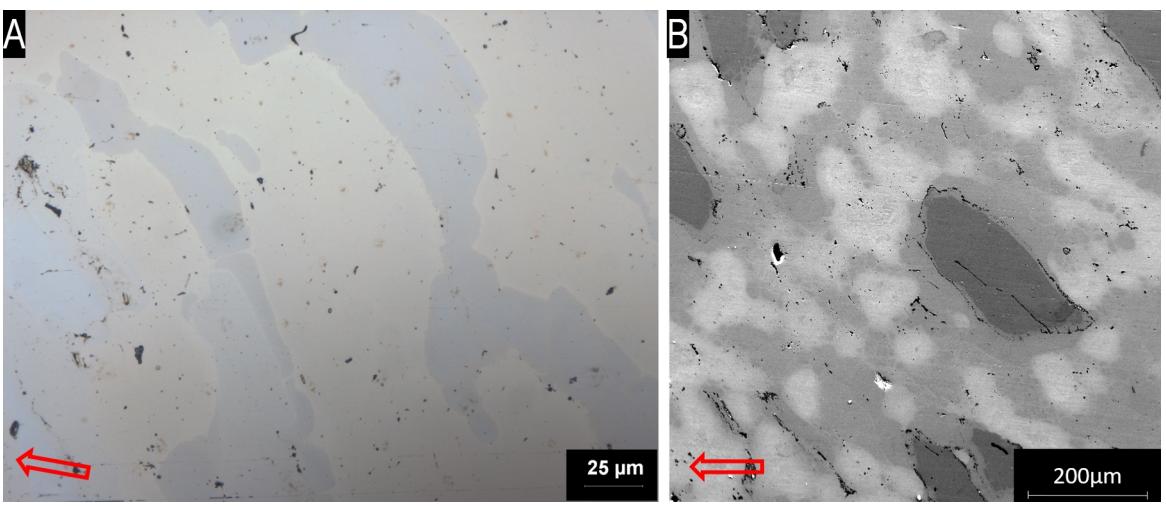

Figure 7. Optical (A) and electron (B) microscopy micrographs for the sample subjected to one ECAP pass, after heat treatment.

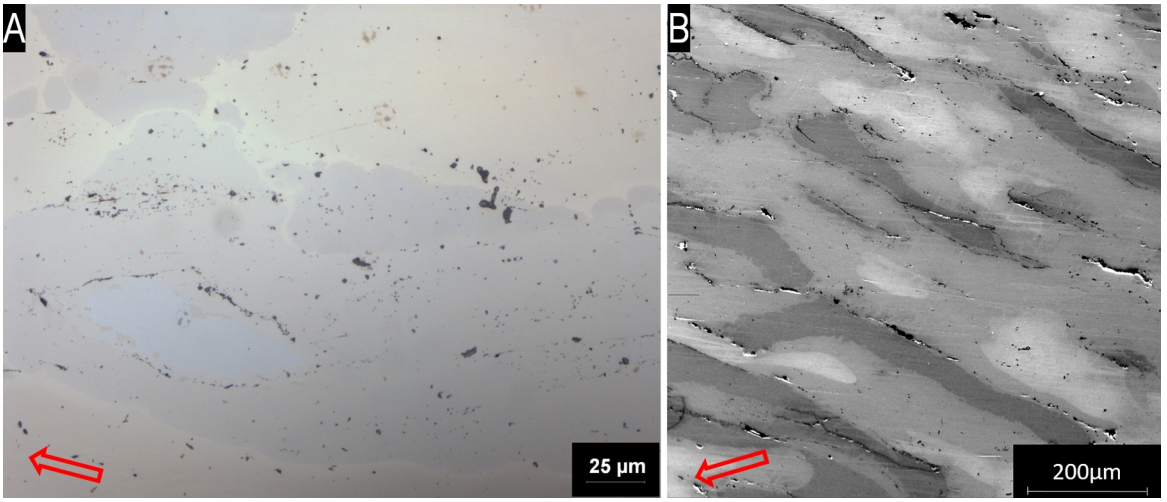

Figure 8. Optical (A) and electron (B) microscopy micrographs for the sample subjected to two ECAP passes, after heat treatment.

Table 1. Calculated volumetric fraction of porosities for samples before and after heat treatment.

	Number of passes	Volumetric fraction of porosities (%)
Untreated	1 pass	2.77 ± 0.51
	2 passes	1.57 ± 0.18
Heat treated	1 pass	1.05 ± 0.17
	2 passes	0.86 ± 0.26

SEM-EDX maps for the first and second pass samples before heat treatment are shown in Figures 9 and 10. By analyzing Figure 9 and Figure 10, it can be observed that the SPD provided by ECAP, solely, did not induce substantial mass transfer between particles. A close agreement was observed between SEM-EDX maps and line scans (Figures. 13 and 14) in the interfaces between particles in one and two passes.

Interface diffusion during ECAP consolidation has already been observed by Ng and collaborators[26] by STEM-EDX in distances of approximately 10 nm in similar processing of Ti-6Al-4V at 400 °C. An initial analysis about the feasibility of diffusion between two metallic particles would conclude that surface oxide layer would suppress mass transfer. However, ECAP processing, leads to shattering of the surface oxide layer of particles, once it cannot be plastically deformed, as

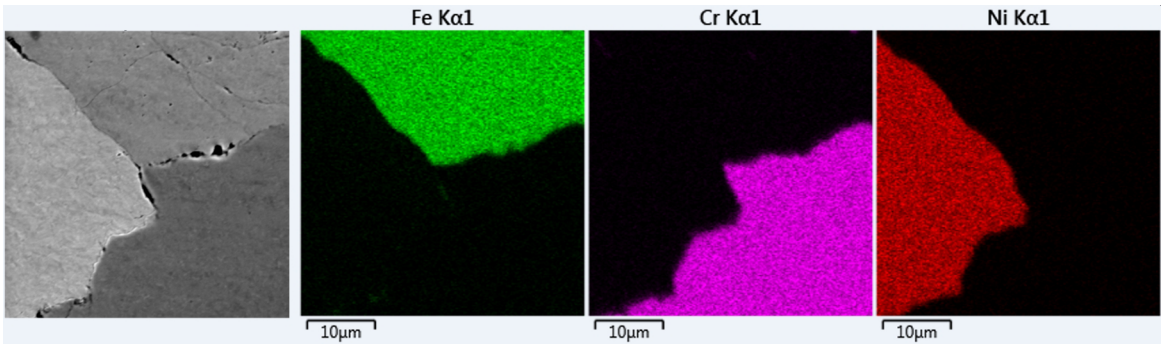

Figure 9. SEM-EDX maps for the sample subjected to one ECAP pass, before heat treatment.

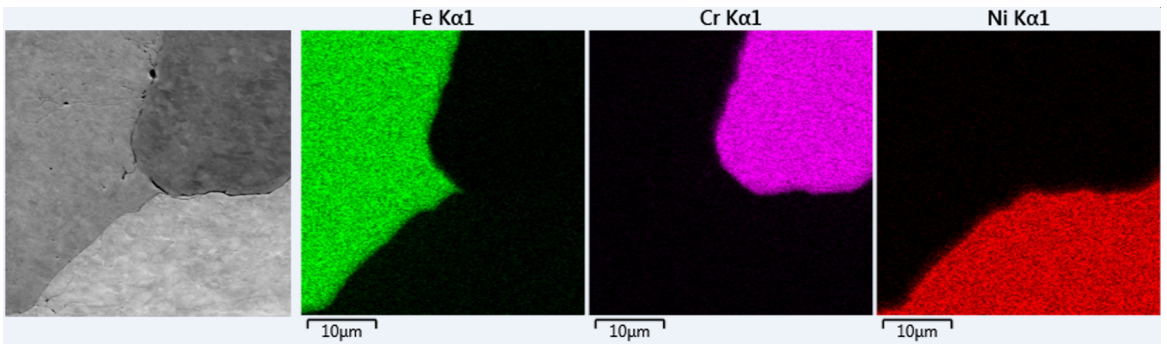

Figure 10. SEM-EDX maps for the sample subjected to two ECAP passes, before heat treatment.

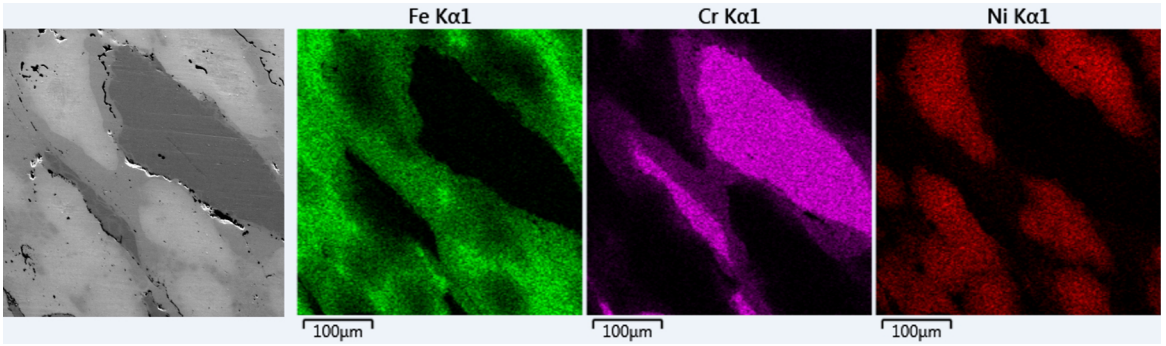

Figure 11. SEM-EDX maps for the sample subjected to one ECAP pass, after heat treatment.

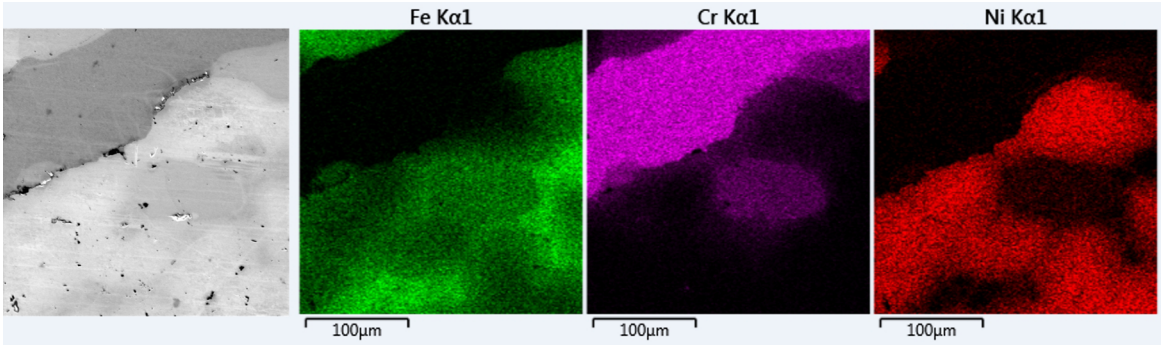

Figure 12. SEM-EDX maps for the sample subjected to two ECAP passes, after heat treatment.

the particle itself[16]. When not completely withdrawn, oxides will be a barrier for mass transfer; but Ng[26] have found that ECAP processing leads to the amorphization of these oxides, which could possibly be less restrictive for diffusion than crystalline oxides.

Additionally, Ahn and collaborators[30,31] reported the formation of intermetallics of Al and Mg after 10 turns HPT of stacked disks of these elements at room temperature, which indicates that interdiffusion between different particles may be induced by this SPD method.

SEM-EDX maps for the first and second pass after heat treatment are shown in Figures 11 and 12, respectively, and present evidences that interdiffusion has happened along the analyzed area during heat treatment. In both figures, it can be observed that the interfaces between particles are not well defined, but composed of a compositional gradient due to interdiffusion between particles. The results on these figures confirms that heat treatment is indeed necessary for achieving substantial mass transfer between particles. Once again, SEM-EDX line scans were performed to further investigate the interfaces, as can be observed in Figures 15 and 16.

SEM-EDX maps and line scans of the heat treated samples evidenced a pattern where the diffusivity of the elements depends on the diffusion pair to which it was subjected. According to the maps, Fe diffusion was more efficient in Ni than in Cr; Cr diffusion was more efficient in Fe than in Ni; and Ni diffusion was rather inefficient in Cr, but some diffusion to Fe particles was observed. This result corroborated the finding of Million, Růžičková and Vřešťál on the self-diffusion coefficients of the Fe-Cr-Ni ternary system[32]. According to those authors, for a large range of temperatures and concentrations, $D_{Ni}^{*} : D_{Fe}^{*} : D_{Cr}^{*} = 1 : 1.2 : 2$.

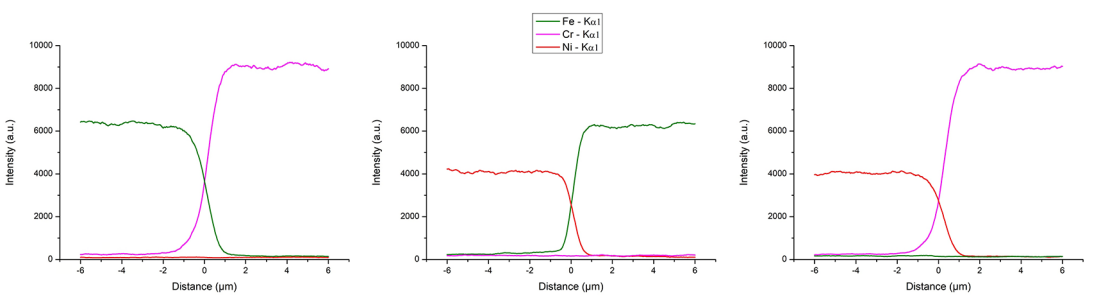

Figure 13. SEM-EDX line scans for the interfaces between particles on the sample subjected to one ECAP pass, before heat treatment.

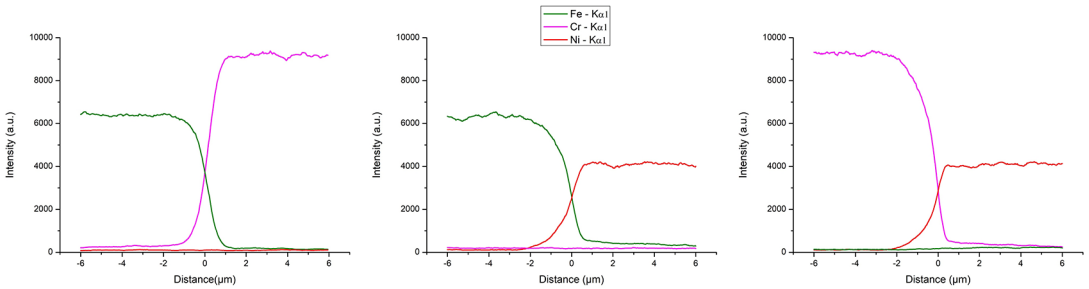

Figure 14. SEM-EDX line scans for the interfaces between particles on the sample subjected to two ECAP passes, before heat treatment

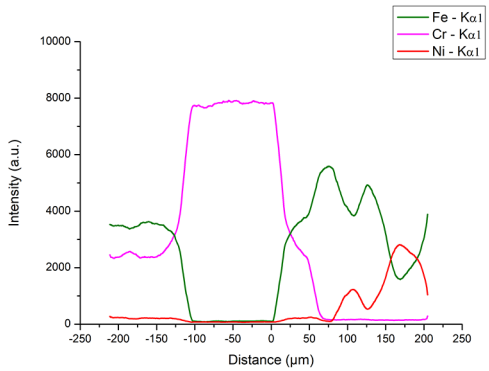

Figure 15. SEM-EDX line scans for the interfaces between particles on the sample subjected to one ECAP pass, after heat treatment.

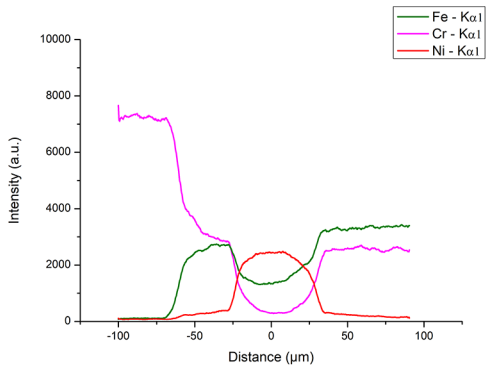

Figure 16. SEM-EDX line scans for the interfaces between particles on the sample subjected to two ECAP passes, after heat treatment.

In order to better understand the interdiffusion behavior during the heat treatment, one-dimensional diffusion simulations were performed using DICTRA (Thermo-Calc - Limited Version 2019a) in conjunction with the thermodynamic database FEDEMO and the mobility database MFEDEMO. The simulations were made considering planar geometry, a 50 μm region for each element, 50 points (linear grid) per region, and a thermal profile identical to the experimental heat treatment (1 h at 1200 °C). Figure 17A and 17B show the composition profile across Fe-Ni and Fe-Cr interfaces, respectively. At the starting time (zero seconds), one has a pure iron particle in contact with a pure nickel/chromium particle. The Fe and Ni particles are FCC, while Cr is BCC. After the complete heat treatment (3600 seconds), the amount of interdiffusion between the Fe-Ni particles is very limited, reaching less than 20 μm inwards the Fe particle. Differently, there is a large mass transfer from the Cr particle inwards the Fe particle, reaching the whole 50 μm region. These results are in great concordance with the SEM-EDX line profiles (Figures 15 and 16), that show some regions with high Fe and Cr concentrations (prior Fe particles) and others with high Cr and very low Fe (prior Cr particles). An explanation for the high Cr diffusion into the Fe structure is the austenite destabilization caused by the Cr enrichment, as the diffusion coefficients of substitutional impurities are at least one order of magnitude higher for BCC iron than for FCC iron[33]. As seen in Figure 17C, the width of the FCC regions shortens as the Cr content increases during the heat treatment. Effectively, the entire Fe region is BCC after 1050 seconds of heat treatment. Important to notice that this is a simplified analysis, considering only the diffusion of a single solute species into the Fe particle. Although this is a reasonable approximation for short heat treatments, the real interdiffusion process, especially for longer heat treatments (which would promote a greater homogenization and interactions between Cr and Ni atoms), would be significantly more complex.

Fiebig and Amouyal[34,35] have demonstrated that SPD processing may create preferential, high speed, diffusion paths in bulk metals which may justify why the sample subjected to a second pass showed a more substantial interdiffusion between these particles.

3.5 Hardness tests

Vickers hardness tests were performed in the powder prior to consolidation and after 1 and 2 passes. Results are displayed in Table 2.

The hardness for Mn particles after consolidation was not included due to small amount and the possible detachment of the particles during sample preparation. The initial Mn powder presented a hardness of about 247.4 ± 23.1 HV.

According to Table 2, Fe and Ni powders present similar hardness prior to consolidation, around 130 HV. Cr particles, on the other hand, presented a higher hardness

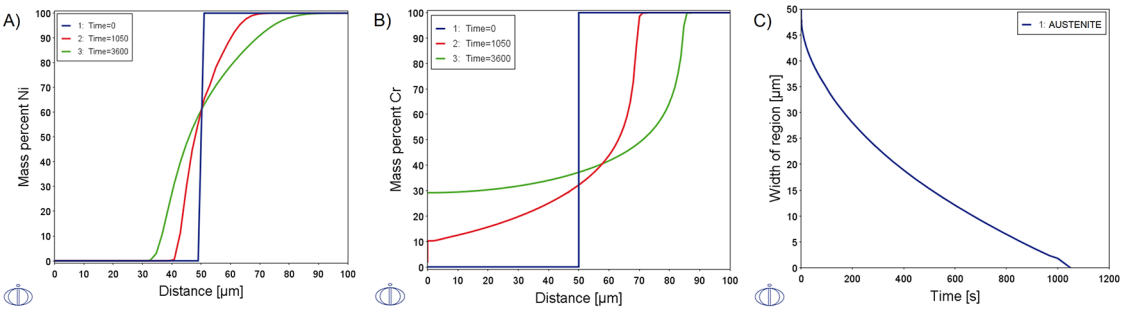

Figure 17. Simulated composition profile across Fe-Ni (A) and Fe-Cr (B) interfaces. The destabilization of austenite caused by Cr enrichment by interdiffusion is displayed in (C).

of 272 HV. After the first and second ECAP passes, all powders presented a substantial hardness increase. This increase was mostly observed during the first pass, which possibly consumed, in great amount, the work-hardening capacity of the metals.

A hardness increase of 272% was observed for Ni after the first ECAP pass, as well as 196% and 125% for Fe and Cr, respectively. A hardness increase of 294% was observed for Ni after 2 ECAP passes, as well as 205% and 138% for Fe and Cr, respectively. This difference can be associated, primarily, to the moderately high stacking fault (128 mJm^{-2}) FCC structure of Ni, which is highly prone to work-hardening when compared to the BCC structure of Fe and Cr[36].

Independently of the material, it was seen that ECAP processing was successful on producing a harder material, which means that all metals underwent an appreciable level of deformation. Thus, this deformation may have led to a substantial refinement on its microstructure and a pronounced increase in dislocation density. Due to the dissimilar nature of the samples, revealing the individual particles microstructure by etching was not possible.

After heat treatment, hardness measurements were performed with higher loads (about 500 gf), since it was not possible to easily distinguish between the particles of different elements. Thus, the measurements were made in order to obtain information about a large area of the sample, comprising several particles. The average hardness of both samples was considerably lower than the particles before heat treatment, indicating that the heat treatment led to an efficient stress relief on the samples. The hardness after heat treatment was even lower than the average hardness of the powders prior to ECAP. After heat treatment, the samples with 2 passes presented a higher hardness than the sample with a single pass. This is probably caused by a more refined recrystallized microstructure in this sample. Larger amounts of plastic deformation increase the number of effective recrystallization nuclei, leading to smaller grains (35,36). It is also possible that the higher hardness is linked to an increased solid solution due to a larger interdiffusion of elements. Although some solid solution hardening is surely present after heat treatment; it is not possible to predicate its influence by Vickers hardness solely.

4. Conclusions

ECAP consolidation of blended elemental powders of Fe, Cr, Ni and Mn, at room temperature, was successfully performed for obtaining a bulk highly dense material.

Good densification was obtained in a single pass of ECAP consolidation. Additional passes led to an improvement in densification and metal-metal bonding in the interfaces between particles.

SEM-EDX analysis demonstrated that mechanical alloying was not, initially, possible by ECAP consolidation solely. However, heat treatment of samples showed that interdiffusion of elements can lead to alloying, especially after higher ECAP strains.

Hardness tests indicated that ECAP consolidation may produce harder materials by work hardening.

Table 2. Vickers hardness for powders before and after ECAP, and bulk Vickers hardness of samples after

	Number of passes	Fe (HV)	Cr (HV)	Ni (HV)
Powders (as received)		129.5 ± 7.9	272.75 ± 20.1	132.7 ± 10.4
Untreated	1 pass	253.3 ± 8.9	340.3 ± 10.3	361 ± 7.5
	2 passes	265 ± 4.9	376.5 ± 6.78	390.3 ± 11.4
			Bulk (HV)	
Heat treated	1 pass		112.8 ± 7.3	
	2 passes		126.7 ± 7.1	

5. Acknowledgements

The author RSN acknowledges Coordenação de Aperfeiçoamento de Pessoal de Nível Superior - Brasil (CAPES) for the scholarship.

The authors LMF, ACKF and AGB acknowledge Fundação Araucária for the scholarship.

The authors would like to express their deepest condolences for the loss of Lorena Moraes Feitosa, a good friend and a promising researcher. She will be missed very much.

6. References

1. Valiev RZ, Islamgaliev RK, Alexandrov IV. Bulk nanostructured materials from severe plastic deformation. *Progress in Materials Science*. 2000;45:103-189.

2. Valiev RZ, Korznikov AV, Mulyukov RR. Structure and properties of ultrafine-grained materials produced by severe plastic deformation. *Materials Science and Engineering: A*. 1993;168(2):141-148.

3. Iwahashi Y, Wang J, Horita Z, Nemoto M, Langdon TG. Principle of equal-channel angular pressing for the processing of ultra-fine grained materials. *Scripta Materialia*. 1996;35(2):143-146.

4. Azushima A, Kopp R, Korhonen A, Yang DY, Micari F, Lahoti GD, et al. Severe plastic deformation (SPD) processes for metals. *CIRP Annals – Manufacturing Technology*. 2008;57(2):716-735.

5. Edalati K, Horita Z. A review on high-pressure torsion (HPT) from 1935 to 1988. *Materials Science and Engineering: A*. 2016;652:325-352.

6. Saito Y, Utsonomiya H, Tsuji N, Sakai T. Novel ultra-high straining process for bulk materials – Development of the accumulative roll-bonding (ARB) process. *Acta Materialia*. 1999;47(2):579-583.

7. Furukawa M, Iwahashi Y, Horita Z, Nemoto M, Langdon TG. The shearing characteristics associated with equal-channel angular pressing. *Materials Science and Engineering: A*. 1998;257(2):328-332.

8. Segal VM, Reznikov VI, Drobyshevskiy AE, Kopylov VI. Plastic working of metals by simple shear. *Russian Metallurgy*. 1981;1:99-105.

9. Segal VM. Materials processing by simple shear. *Materials Science and Engineering: A*. 1995;197(2):157-164.

10. Segal VM. Equal channel angular extrusion: from macromechanics to structure formation. *Materials Science and Engineering: A*. 1999;271:322-333.

11. Valiev RZ, Langdon TG. Principles of equal-channel angular pressing as a processing tool for grain refinement. *Progress in Materials Science*. 2006;51(7):881-981.

12. Mendes Filho AA, Prados EF, Valio GT, Rubert JB, Sordi VL, Ferrante M. Severe plastic deformation by equal channel angular pressing: product quality and operational details. *Materials Research*. 2011;14(3):335-339.

13. Manjunath GK, Kumar GVP, Bhat KU, Huilgol P. Microstructure and mechanical properties of cast Al-5Zn-2Mg alloy subjected to equal-channel angular pressing. *Journal of Materials Engineering and Performance*. 2018;27(11):5644-5655.

14. Manjunath GK, Kumar GVP, Bhat KU. Tensile properties and tensile fracture characteristics of cast Al-Zn-Mg alloys processed by equal channel angular pressing. *Transactions of the Indian Institute of Metals*. 2017;70(3):833-842.

15. Haghighi RD, Jahromi S, Moresedgh A, Tabandeh-Khorsid M. A comparison between ECAP and conventional extrusion for consolidation of aluminum matrix composite. *Journal of Materials Engineering and Performance*. 2012;21(9):1885-1892.

16. Xia K. Consolidation of particles by severe plastic deformation: mechanism and applications in processing bulk ultrafine and nanostructured alloys and composites. *Advanced Engineering Materials*. 2010;12(8):724-729.

17. Lapovok R, Tomus D, Muddle BC. Low-temperature compaction of Ti-6Al-4V powder using equal channel angular extrusion with backpressure. *Materials Science and Engineering: A*. 2008;490:171-180.

18. Parasiris A, Hartwig KT. Consolidation of advanced WC-Co powders. *International Journal of Refractory Metals and Hard Materials*. 2000;18(1):23-31.

19. Munir ZA. Surface oxides and sintering of metals. *Powder Metallurgy*. 1981;24(4):177-180.

20. Ribeiro MP, Hupalo MF, Vurobi Junior S, Cintho OM. Study of sintering iron powder bars processed by equal channel angular pressing. *Materials Science Forum*. 2014;802:404-408.

21. Xia K, Wu X. Back pressure equal channel angular consolidation of pure Al particles. *Scripta Materialia*. 2005;53(11):1225-1229.

22. Xia K, Wu X, Honma T, Ringer S. Ultrafine pure aluminium through back pressure equal channel angular pressing (BP-ECAP) of particles. *Journal of Materials Science*. 2007;42(5):1551-1560.

23. Haouaoui M, Karaman I, Maier HJ, Hartwig KT. Microstructure evolution and mechanical behavor of bulk copper obtained by consolidation of micro and nanopowders using equal channel angular pressing. *Metallurgical and Materials Transactions: A*. 2004;35(9):2935-2949.

24. Karaman I, Robertson JD, Im JT, Mathaudhu SN, Luo ZP, Hartwig KT. The effect of temperature and extrusion speed on the consolidation of zirconium-based metallic glass powder using equal-channel angular extrusion. *Metallurgical and Materials Transactions: A*. 2004;35(1):247-256.

25. Cubero-Sesin JM, Horita Z. Powder consolidation of Al-10wt%Fe alloy by high-pressure torsion. *Materials Science and Engineering: A*. 2012;558:462-471.

26. Ng HP, Haase C, Lapovok R, Estrin Y. Improving sinterability of Ti-6Al-4V from blended elemental powders through equal channel angular pressing. *Materials Science and Engineering: A*. 2013;565:396-404.

27. Yamaguchi D, Horita Z, Nemoto M, Langdon TG. Significance of adiabatic heating in equal channel angular pressing. *Scripta Materialia*. 1999;41(8):791-796.

28. American Society for Testing and Materials (ASTM). *E1245-03 – Standard practice for determining the inclusion or second-phase constituent content of metals by automatic image analysis*. West Conshohocken, PA: ASTM International; 2016.

29. Valiev RZ, Alexandrov IV, Zhu YT, Lowe TC. Paradox of strength and ductility in metals processed by severe plastic deformation. *Journal of Materials Research*. 2002;17(1):5-8.

30. Ahn B, Lee HJ, Choi IC, Kawasaki M, Jang JI, Langdon TG. Micro-mechanical behaviour of an exceptionally strong metal matrix nanocomposite processed by high-pressure torsion. *Advanced Engineering Materials*. 2016;18:1001-1008.

31. Ahn B, Zhilyaev AP, Lee HJ, Kawasaki M, Langdon TG. Rapid synthesis of an extra hard metal matrix nanocomposite at ambient temperature. *Materials Science and Engineering: A*. 2015;635:109-117.

32. Million B, Růžičková J, Vřešál J. Diffusion in Fe-Ni-Cr alloys with an F.C.C. lattice. *Materials Science and Engineering: A*. 1985;72(1):85-100.

33. Mehrer H. *Diffusion in solids: fundamentals, methods, materials, diffusion-controlled processes*. Berlin: Springer-Verlag; 2007.

34. Fiebig J, Divinski S, Rosner H, Estrin Y, Wilde G. Diffusion of Ag and Co in ultrafine-grained α-Ti deformed by equal channel angular pressing. *Journal of Applied Physics*. 2011;110:083514.

35. Amouyal Y, Divinski SV, Estrin Y, Rabkin E. Short-circuit diffusion in an ultrafine-grained copper-zirconium alloy produced by equal channel angular pressing. *Acta Materialia*. 2007;55(17):5968-5979.

36. Humphreys FJ, Hatherly M. *Recrystallization and related annealing phenomena*. 2nd ed. Oxford: Pergamon; 2004.